eScience 2 (2022) 183–191

Contents lists available at ScienceDirect

eScience

journal homepage: www.keaipublishing.com/en/journals/escience

Research Paper

Probing thermally-induced structural evolution during the synthesis of layered Li-, Na-, or K-containing 3*d* transition-metal oxides

Weibo Hua [a,b,*], Xiaoxia Yang [a], Nicola P.M. Casati [d], Laijun Liu [c], Suning Wang [a,b,c,*], Volodymyr Baran [e], Michael Knapp [b], Helmut Ehrenberg [b], Sylvio Indris [b,*]

[a] School of Chemical Engineering and Technology, Xi'an Jiaotong University, Xi'an, Shaanxi, 710049, China
[b] Institute for Applied Materials (IAM), Karlsruhe Institute of Technology (KIT), Hermann-von-Helmholtz-Platz 1, D-76344, Eggenstein-Leopoldshafen, Germany
[c] College of Materials Science and Engineering, Guilin University of Technology, Guilin, 541004, China
[d] Paul Scherrer Institut (PSI), WLGA/229, 5232, Villigen PSI, Switzerland
[e] Deutsches Elektronen-Synchrotron (DESY), Notkestr. 85, Hamburg, 22607, Germany

HIGHLIGHTS

- *In situ* high-resolution HT-sXRD techniques was used to unveil the Li/Na/K-ion insertion induced structural evolution during heating.
- The dynamics of chemical reaction between alkali-free precursor and alkali species upon calcination were systematically investigated.
- High-temperature lithiation reaction pathway strongly depends on the alkali-free precursor type.
- Site preferences of Li/Na/K-ion leads to the formation of various types of layered structures.

GRAPHICAL ABSTRACT

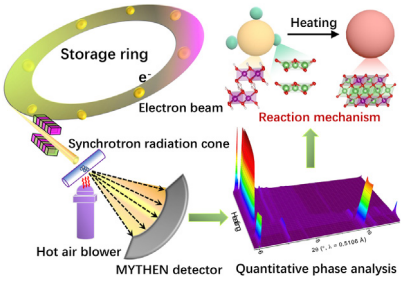

ARTICLE INFO

Keywords:
In situ sXRD
Structural evolution
3d transition-metal oxides
Layered structure
High-temperature solid-state reaction

ABSTRACT

Layered alkali-containing 3*d* transition-metal oxides are of the utmost importance in the use of electrode materials for advanced energy storage applications such as Li-, Na-, or K-ion batteries. A significant challenge in the field of materials chemistry is understanding the dynamics of the chemical reactions between alkali-free precursors and alkali species during the synthesis of these compounds. In this study, in situ high-resolution synchrotron-based X-ray diffraction was applied to reveal the Li/Na/K-ion insertion-induced structural transformation mechanism during high-temperature solid-state reaction. The in situ diffraction results demonstrate that the chemical reaction pathway strongly depends on the alkali-free precursor type, which is a structural matrix enabling phase transitions. Quantitative phase analysis identifies for the first time the decomposition of lithium sources as the most critical factor for the formation of metastable intermediates or impurities during the entire process of Li-rich layered $Li[Li_{0.2}Ni_{0.2}Mn_{0.6}]O_2$ formation. Since the alkali ions have different ionic radii, Na/K ions tend to be located on prismatic sites in the defective layered structure ($Na_{2/3-x}[Ni_{0.25}Mn_{0.75}]O_2$ or $K_{2/3-x}[Ni_{0.25}Mn_{0.75}]O_2$) during calcination, whereas the Li ions prefer to be localized on the tetrahedral and/or octahedral sites, forming O-type structures.

* Corresponding authors.
E-mail addresses: weibo.hua@xjtu.edu.cn (W. Hua), suning.wang@xjtu.edu.cn (S. Wang), sylvio.indris@kit.edu (S. Indris).

https://doi.org/10.1016/j.esci.2022.02.007
Received 13 December 2021; Received in revised form 16 January 2022; Accepted 22 February 2022
Available online 7 March 2022

1. Introduction

At present, the solid-state reaction plays an important role in various areas of science, such as solid-state physics [1–3], chemistry [4–6], materials science [4,7,8], and electrochemistry [8–10]. To achieve the rational synthesis of target materials, unravelling the competition between the thermodynamics and kinetics of solid-state reactions is of great significance. Thermodynamics deals with the study of the formation enthalpies of all possible formed phases for a given overall composition, and thus, the choice of target materials does not depend on the reaction pathway. Kinetics is concerned with the activation energy barriers of the reaction steps, which determines the rate of formation of intermediate and final compounds. In the synthesis of inorganic materials, the solid-state reaction usually proceeds through multiple steps, with the concurrent formation of nonequilibrium intermediates before the generation of the target materials [11]. These reactions generally yield non-equilibrium kinetic side products rather than the thermodynamic equilibrium substances [4]. Exploration of the reaction pathway and structural evolution during the synthesis of the desired materials is therefore critical.

The high-temperature solid-state reaction between 3*d* transition-metal (TM) oxides and alkali (Li/Na/K) species under an air/oxygen atmosphere is widely utilized for the production of alkali-containing transition-metal oxides (ATMOs) [12–14]. In recent decades, ATMOs have attracted broad interest and sparked intensive investigations of these compounds as cathode materials for secondary batteries [15–25]. For instance, Li- and Mn-rich layered oxides (LMROs) are among the most promising cathode materials for next-generation Li-ion batteries, owing to their high specific capacities (over 250 mAh g^{-1}) and low cost [26–28]. It is well known that the synthetic process has a great influence on the structure and chemical composition of LMROs, which, in turn, affect the electrochemical performance considerably [29–32]. Two interesting questions that need to be explained are (i) whether the high-temperature lithiation reaction is kinetically or thermodynamically controlled, and (ii) whether there is a universal reaction pathway in the process of ATMOs formation using various precursor types.

Recently, several advanced synchrotron-based techniques [33] have been used to elucidate the formation mechanism during the synthesis of layered ATMOs for practical purposes, including synchrotron-based X-ray diffraction (sXRD) [34,35], X-ray absorption spectroscopy (XAS) [30,36], and pair distribution function (PDF) analysis [37,38]. Among these, time-resolved high-resolution sXRD is the most powerful tool to monitor the long-range structural changes occurring in bulk materials, due to its high sensitivity and fast data acquisition (i.e., hundreds of sXRD patterns within 2 h) [39–42]. For instance, a series of fast non-equilibrium phase transformations (i.e., metastable layered O3, O3′, and P3 phases) during the process of P2-type Na_xCoO_2 formation were reported by Wang's group [21]. They found that even though the P2-type structure is the equilibrium phase, compositionally unconstrained reactions between reactants facilitate the formation of non-equilibrium intermediates.

Our previous work [43] revealed that a mixture of Li-free compounds and lithium sources successively becomes a kind of activated complex with a spinel ($Fd\bar{3}m$) and/or rock-salt-type ($Fm\bar{3}m$) structure that eventually transforms into Li-containing layered Li(Ni,Co,Mn)O_2 oxides ($R\bar{3}m$), accompanied by Li/O incorporation and crystal growth. Unfortunately, unravelling the Li/Na/K-ion insertion-induced structural evolution during the synthesis of ATMOs poses challenging hurdles because (a) the reaction process at high temperature is too fast to be followed in real time by conventional devices such as laboratory XRD; and (b) it is difficult to probe the crystallographic information of low-Z alkali elements such as lithium (because of the low electron density around these atoms).

In this study, we used in situ high-temperature sXRD (HT-sXRD) to systematically examine the solid-state reaction mechanism of Li/Na/K insertion into alkali-free compounds. Three different precursors — Li-free transition-metal hydroxide, carbonate, and spinel oxide — were chosen as starting materials to investigate the influence of precursor type on the high-temperature lithiation reaction pathway. The nuances of chemical reactions between spinel $Mn[Ni_{0.75}Mn_{1.25}]O_4$ ($Fd\bar{3}m$) and $LiOH{\cdot}H_2O$ under isothermal heat treatment were carefully analyzed and compared. Very importantly, Li species could react with CO_2, forming Li_2CO_3 at high temperature (100–700 °C) and in the presence of air, playing a peculiar role in the formation of intermediates during the synthesis of Li-rich layered $Li[Li_{0.2}Ni_{0.2}Mn_{0.6}]O_2$ (*C2/m*). To check whether this reaction with lithium in the formation mechanism of ternary oxides also has high relevance for the design and synthesis of Na/K-containing layered oxides, we again used in situ HT-sXRD to observe the structural evolution of mixtures of spinel $Mn[Ni_{0.75}Mn_{1.25}]O_4$ and Na_2CO_3 or K_2CO_3 during continuous heating. Our results offer new insights into the high-temperature solid-state reaction mechanisms during Li/Na/K-ion insertion and the limitations of these reaction kinetics, which might open a new avenue in the synthetic design of advanced electrode materials for a wide range of applications in electrical energy storage devices.

2. Results and discussion

In situ HT-sXRD was firstly carried out to investigate the structural evolution and phase transformation mechanism of a mixture of the precursor and lithium source during the synthesis of cobalt-free layered $Li[Li_{0.2}Ni_{0.2}Mn_{0.6}]O_2$ (Li[Li,TM]O_2, LLNMO). Each diffraction pattern was analyzed using the Rietveld refinement method described in this work (see the Supporting Information). Fig. 1a and Fig. S1 show the in situ HT-sXRD patterns of a blend of oxyhydroxide precursor (TMOOH) and lithium hydroxide during heating (90–750 °C). At lower temperatures (less than 100 °C), the main reflections were assigned to a layered TMOOH (*C2/m*) [44] and a tetragonal LiOH (*P4/nmm*).

As the temperature increased to 500 °C, the reflections indexed to TMOOH and LiOH gradually disappeared, and a set of new reflections progressively appeared, including 001_m at 6.1°, 130_m at 11.8°, and $\bar{1}\,31_m$ at 12.3°, belonging to a monoclinic layered Li(Li,TM)O_2 (*C2/m*). In addition, a minor phase assigned to a Li-containing rock-salt-type disordered $[Li_xTM_{(1-x)}]O$ ($Fm\bar{3}m$) was also observed. The weight fractions of the rock-salt-type $[Li_xTM_{(1-x)}]O$ phase and the layered LLNMO phase were estimated to be 20.0(7) wt% and 80.0(7) wt% from pattern 6 after 40 min at 500 °C, as exhibited in Fig. 1b.

When the temperature was above 700 °C, the rock-salt-type $[Li_xTM_{(1-x)}]O$ phase successively transformed to the monoclinic layered LLNMO. Noticeably, the generation of LLNMO at around 500 °C indicated the occurrence of the Li^+/H^+-ion exchange reaction, presented in reaction 1, where Δ represents calcination conditions (see Fig. 1c):

$$\mathrm{TMOOH} + \mathrm{Li}^+ \xrightarrow{\Delta} \mathrm{Li(TM)O_2} + \mathrm{H}^+ \quad (1)$$

Interestingly, no reflections corresponding to the Li_2CO_3 phase were observed in the in situ HT-sXRD patterns; this suggested the Li ions had been inserted into the interior structure, resulting in the generation of layered Li[Li,TM]O_2 at a relatively low temperature (500 °C) through a Li^+/H^+-ion exchange reaction. In other words, there was no Li source on the crystallites' surface reacting with CO_2 along this reaction path. On the basis of the in situ HT-sXRD results and our previous work [25,27–44], we propose a possible reaction mechanism and structural evolution for the formation of LLNMO during heating, shown in Fig. 1c.

HT-sXRD was also used to trace the reaction mechanism between the carbonate precursor ($TMCO_3$) and Li source (LiOH) during thermal treatment. As presented in Fig. 2a and Fig. S2, when the temperature increased to approximately 250 °C, the $TMCO_3$ gradually transformed to a cubic rock-salt TMO ($Fm\bar{3}m$), as evidenced by the appearance of a new 111_r reflection at 11.6°, accompanied by the release of CO_2. Simultaneously, a set of new reflections was found in the sXRD patterns: 110 at

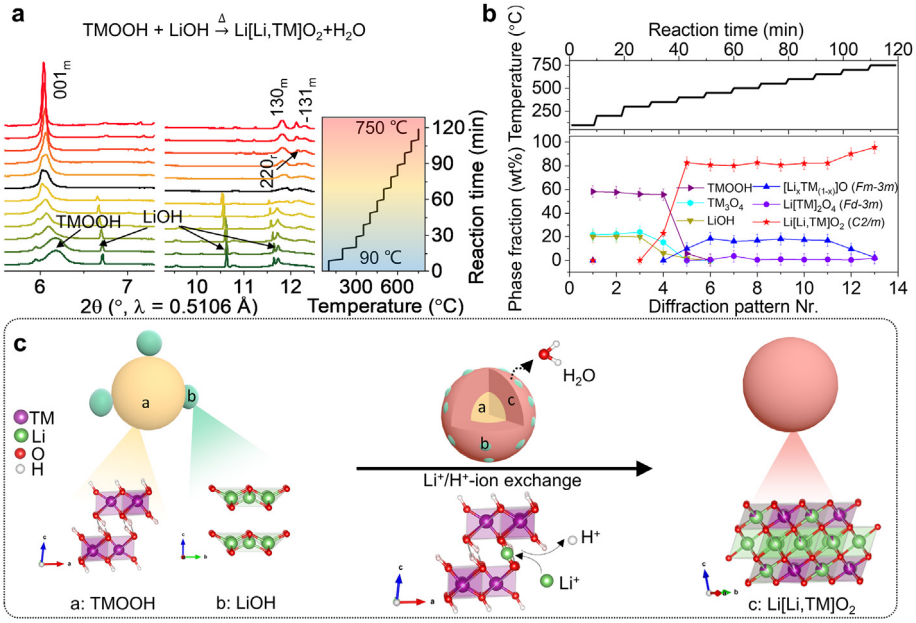

Fig. 1. (a) In situ HT-sXRD patterns and (b) the corresponding phase fraction evolution of a mixture of the precursor TMOOH and LiOH during high-temperature reaction from 90 to 750 °C; subindices r and m at the reflections *hkl* in (a) refer to the rock-salt phase and the monoclinic layered phase, respectively; (c) schematic diagram of a possible reaction mechanism and structural evolution in the synthesis of LLNMO during annealing, starting from TMOOH and LiOH.

7.0°, $\bar{2}$ 02 at 9.8°, and 002 at 10.1°, corresponding to Li_2CO_3 (*C2/c*). An increased Li_2CO_3 content and a decreased $TMCO_3$ concentration suggested that the CO_2 from the formation of Li_2CO_3 originated from the decomposition of $TMCO_3$. However, CO_2 in the air cannot be ruled out as also contributing to the production of Li_2CO_3.

As the high-temperature lithiation reaction proceeded, the 111_r reflection shifted towards higher two-theta scattering angles, signifying the contraction of the lattice parameters of the cubic rock-salt structure. This shrinkage indicated that the fully disordered $[Li_xTM_{(1-x)}]O$ ($0 \leq x \leq 0.5$) had a tendency toward cation reordering onto two separate layers — a Li layer and a TM layer — and the formation of a thermally stable layered LLNMO [27,45], with some densification due to there being less disorder. Consequently, typical reflections belonging to layered LLNMO (e.g., 001_m and 130_m) emerged with the superstructure due to this disorder-to-order phase transition.

With a further increase in temperature to about 750 °C, the intermediate phases and unreacted lithium species formed layered LLNMO (around 90.2 wt%), Li-containing rock-salt-type $[Li_xTM_{(1-x)}]O$ (around 5.1 wt%), and spinel-type $Li[Ni_{0.5}Mn_{1.5}]O_4$ (around 4.7 wt%), as shown in Fig. 2b. Based on the crystallographic structure of these compounds, the Li content of the layered structures (n_{Li}:$n_{TM} \geq 1$) was higher than that of the spinel and rock-salt structures (n_{Li}:$n_{TM} < 1$). It is therefore reasonable to speculate that the Li-rich layered phases were mainly generated in the near-surface region, in contact with the Li source, while the Li-poor rock-salt-type and/or spinel phases remained in the interior

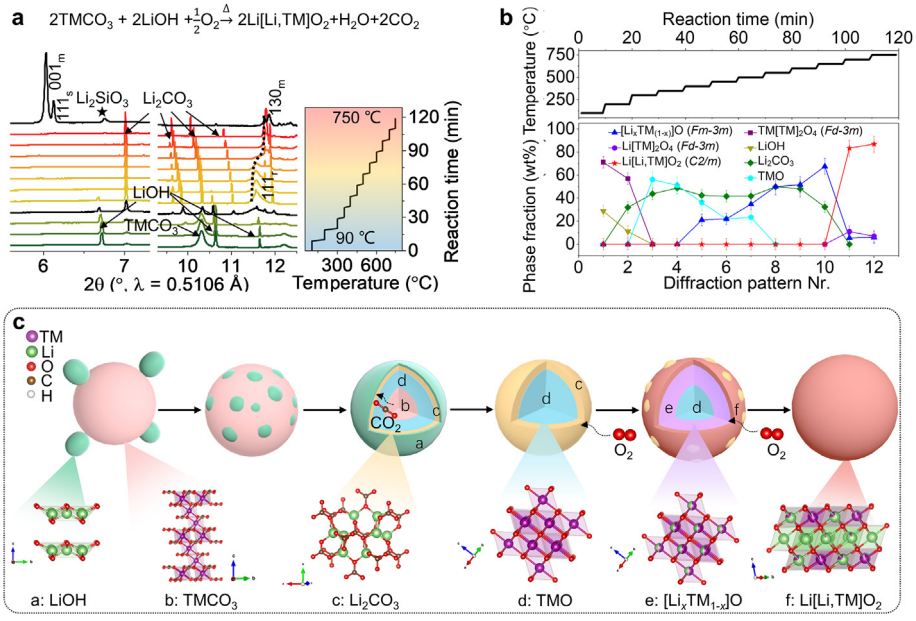

Fig. 2. (a) In situ HT-sXRD patterns and (b) a quantitative analysis of the weight fractions of a mixture of $TMCO_3$ and LiOH during heating from 90 to 750 °C; (c) schematic illustration of a possible reaction mechanism and phase transition for LLNMO formation during heating, starting from $TMCO_3$ and LiOH.

area of the crystallites (see Fig. 2c). Overall, reactions 2–4 can be roughly described as follows:

$$TMCO_3 \xrightarrow{\approx 250\ ^\circ C} TMO + CO_2 \quad (2)$$

$$LiOH + \frac{1}{2}CO_2 \xrightarrow{\approx 250\ ^\circ C} \frac{1}{2}Li_2CO_3 + \frac{1}{2}H_2O \quad (3)$$

$$\frac{4}{5}TMO + \frac{3}{5}Li_2CO_3 + \frac{3}{10}O_2 \xrightarrow{\approx 720\ ^\circ C} Li(Li_{0.2}TM_{0.8})O_2 + \frac{3}{5}CO_2 \quad (4)$$

Since the hydroxide and carbonate precursors would usually convert to lithium-poor spinel intermediates and then to lithium-rich oxides during the high-temperature lithiation reaction, HT-sXRD was conducted to explore the chemical reaction mechanism between the Li-poor spinel phase, $Mn[Ni_{0.75}Mn_{1.25}]O_4$, and the Li source, $LiOH{\cdot}H_2O$, upon annealing with a constant heating rate of 20 °C min^{-1}. LiOH with space group *P4/nmm* formed rapidly at about 100 °C due to the dehydration reaction, as shown in Figs. 3a, and b. The structural evolution of various phases can also be observed in Fig. S3. Simultaneously, a certain amount of Li_2CO_3 (14.4 wt%) was generated at about 120 °C.

With an increase in temperature from 100 to 450 °C, the weight fraction of the LiOH and Li_2CO_3 phases gradually diminished to about 8.0 wt% and 3.0 wt%, respectively, indicating the decomposition of LiOH and Li_2CO_3. The percentage of the spinel-type phase increased to ~94.5 wt%. Such unreasonably high content was due to the fact that sXRD did not allow a reliable determination of the Li content and might not have detected other Li species, such as Li_2O. As the temperature increased to about 550 °C, the reduced intensity of the 220_s reflection in the sXRD pattern (where the subindex s refers to the spinel-type phase) suggested the insertion of Li ions onto the tetrahedral sites in the spinel structure, forming the $Li[Ni_{0.5}Mn_{1.5}]O_4$ phase ($LiTM_2O_4$). The spinel $Li[Ni_{0.5}Mn_{1.5}]O_4$ phase (*Fd*$\bar{3}$*m*) rapidly transformed to the Li-containing rock-salt-type $[Li_xTM_{(1-x)}]O$ phase (*Fm*$\bar{3}$*m*) and Li-rich layered LLNMO phase (*C2/m*) when the temperature was above 600 °C. Reflections at 7.0°, 9.6°, 10.1°, and 10.8° were indexed based on a defective $Li_{2-x}CO_3$ phase and were found in the sXRD patterns between 600 and 720 °C.

The Rietveld refinement results indicated that the lithium vacancy concentration in the $Li_{2-x}CO_3$ phase was around 0.7 (i.e., $Li_{\sim 1.3}CO_3$). As the temperature increased to 723 °C (i.e., the melting point of Li_2CO_3), the rock-salt-type $[Li_xTM_{(1-x)}]O$ phase (*Fm*$\bar{3}$*m*) gradually converted into the Li-rich layered LLNMO phase (*C2/m*) as a result of Li/O incorporation. Therefore, the overall reaction process was:

$$\frac{4}{9}Mn[Ni_{0.75}Mn_{1.25}]O_4 + 2LiOH \cdot H_2O + \frac{5}{18}O_2 \xrightarrow{\Delta} \frac{5}{3}Li[Li_{0.2}Ni_{0.2}Mn_{0.6}]O_2 + 3H_2O \quad (5)$$

Since a cubic close-packed (ccp) oxygen framework was involved during these reactions, the oxygen uptake led to crystal growth (see Fig. 3c).

Considering that LiOH could react with the precursor at a relatively low temperature (< 500 °C) and Li_2CO_3 decomposition occurs at high temperatures (> 700 °C), Li_2CO_3 on its own and a mixture of Li_2CO_3 and $LiOH{\cdot}H_2O$ were used separately as Li sources to explore the formation pathway of LLNMO during thermal treatment. In situ HT-sXRD was performed to decipher the dynamics of the reaction between TM_3O_4 and the lithium sources (Li_2CO_3 and/or $LiOH{\cdot}H_2O$) under isothermal conditions. The reactants were heated to the selected temperatures (i.e., 650, 700, 725, and 750 °C) with a ramping rate of 20 °C min^{-1} and then maintained at this temperature for about 30 min. The two-dimensional contour maps of the reactants' structural evolution — i.e., TM_3O_4 with the lithium sources (both Li_2CO_3 and $LiOH{\cdot}H_2O$) — are displayed in Fig. 4. The corresponding HT-sXRD pattern ranges from 5.5° to 20.5° are displayed in Figs. S4–7. It can be clearly seen from Figs. 4a and e that $LiOH{\cdot}H_2O$ transformed to LiOH at around 100 °C. All the reflections in the sXRD patterns shifted toward lower scattering angles as the temperature increased to 500 °C, manifesting the expansion of the underlying unit cell. At the same time, a defective $Li_{2-x}CO_3$ phase started to form, growing at the expense of Li_2CO_3. In addition, the reflections belonging to LiOH disappeared. These results revealed that a certain amount of lithium ions may have been inserted into the spinel structure, forming the Li-containing spinel $Li[Ni_{0.5}Mn_{1.5}]O_4$ phase, as evidenced by the disappearance of the 220_s reflection at around 9.9° and the appearance of the 111_s reflection at 6.1°.

When the temperature reached 650 °C, a new set of reflections, including 220_r at 20.0°, emerged, related to the disordered Li-containing

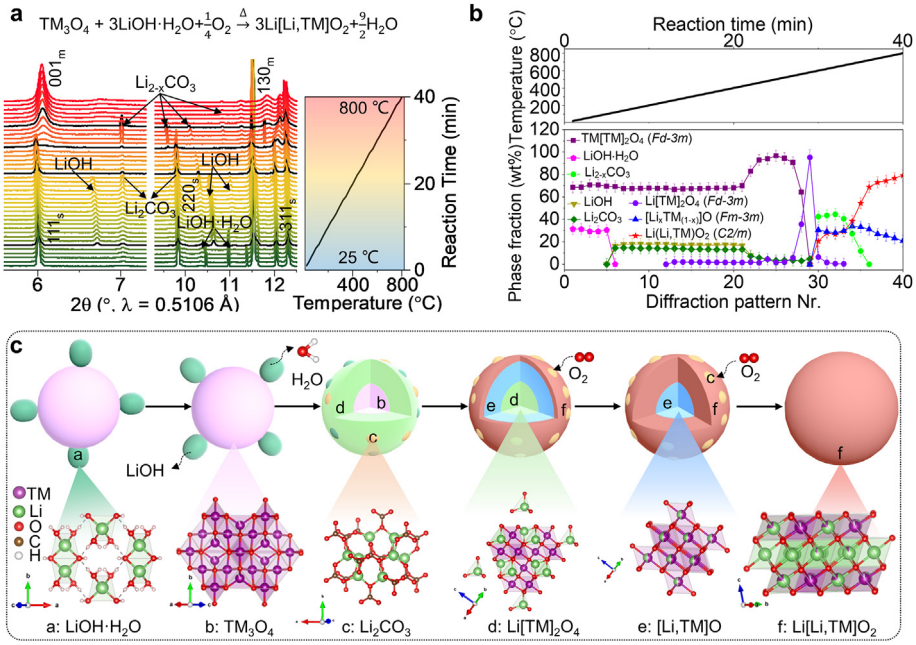

Fig. 3. (a) In situ HT-sXRD pattern of a mixture of spinel $Mn[Ni_{0.75}Mn_{1.25}]O_4$ (TM_3O_4) and $LiOH{\cdot}H_2O$; on the right side next to the sXRD pattern, the corresponding temperature profile during the calcination process is shown; (b) the resulting weight fraction of various phases during calcination between 25 and 800 °C; (c) schematic illustration of a possible reaction mechanism and phase transition for Li-rich layered oxide formation, starting from Li-free spinel oxide and $LiOH{\cdot}H_2O$.

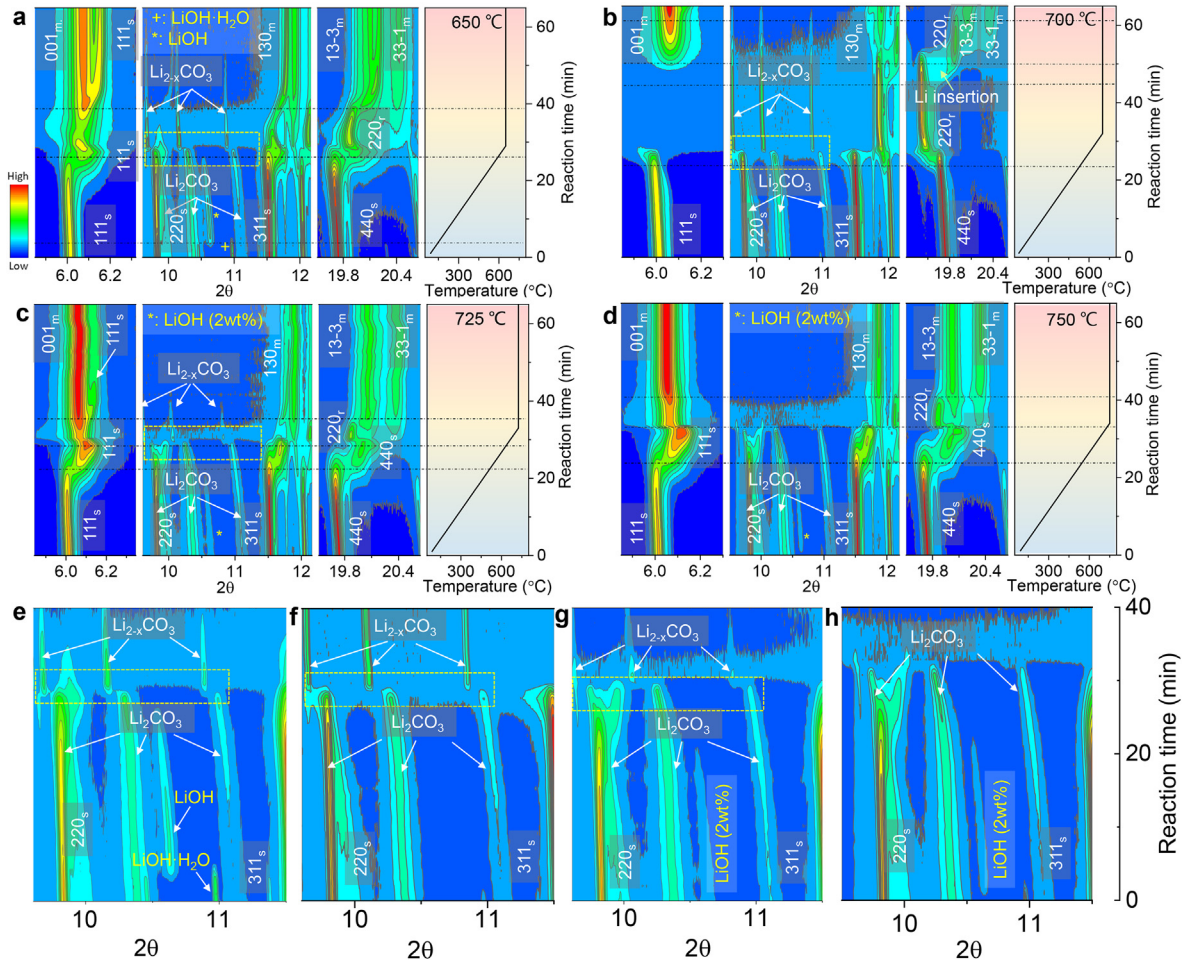

Fig. 4. Contour plots of in situ HT-sXRD patterns of a mixture of TM_3O_4 and a lithium source at (a) 650, (b) 700, (c) 725, and (d) 750 °C, respectively, λ = 0.5106 Å; (e–h) magnification of the region from 9.60 to 11.50°, revealing the changes in Li species during heating. The weight fractions of Li_2CO_3 and $LiOH{\cdot}H_2O$ are 77.0 and 23.0 wt% at 650 °C; the weight fraction of Li_2CO_3 is 100 wt% at 700 °C; the weight fractions of Li_2CO_3 and LiOH are approximately 98.0 and 2.0 wt% at 725 °C and 750 °C, respectively.

rock-salt-type $[Li_xTM_{(1-x)}]O$ phase. As the holding time increased, the defective $Li_{2-x}CO_3$ phase progressively vanished, although the temperature was well below its melting point. This demonstrated that the intermediate cubic phases could accelerate lithium carbonate decomposition [27,44]. On the other hand, the $[Li_xTM_{(1-x)}]O$ phase gradually transformed to the monoclinic layered LLNMO and the spinel $Li[Ni_{0.5}Mn_{1.5}]O_4$ as a consequence of Li/O incorporation. The reflections in the sXRD patterns belonging to the layered LLNMO, spinel $Li[Ni_{0.5}Mn_{1.5}]O_4$, and rock-salt-type $[Li_xTM_{(1-x)}]O$ remained after heating at 650 °C for 1 h, suggesting a three-phase coexistence region in the temperature range from 500 to 650 °C.

When the mixture of spinel TM_3O_4 and Li_2CO_3 was heated to 500 °C (see Figs. 4b and f), the Li_2CO_3 started to become the defective $Li_{2-x}CO_3$ phase, and the spinel TM_3O_4 converted to the rock-salt-type $[Li_xTM_{(1-x)}]O$ phase. The reflection intensity of $Li_{2-x}CO_3$ progressively weakened as the reaction proceeded at 700 °C, suggesting that the disintegration of $Li_{2-x}CO_3$ was thermodynamically favored. Interestingly, a new set of reflections (001_m, 130_m, $13\bar{3}_m$, and $33\bar{1}_m$) occurred simultaneously, illustrating that the Li ions were successively inserted into the fully disordered rock-salt-type $[Li_xTM_{(1-x)}]O$ phase, resulting in the generation of the ordered layered LLNMO superstructure.

Since LiOH can decompose at relatively low temperatures (< 500 °C), a mixture of Li_2CO_3 (~98.0 wt%) and LiOH (~2.0 wt%) was used to study the influence of Li species on the pathway of LLNMO formation. Evidently, the spinel $Li[Ni_{0.5}Mn_{1.5}]O_4$ was formed as the temperature increased to around 600 °C, as shown in Figs. 4c and g. This suggests that LiOH did not react to Li_2CO_3 in air at elevated temperatures but instead reacted with the Li-free spinel TM_3O_4, forming the Li-containing spinel $LiTM_2O_4$, which facilitated the decomposition of Li_2CO_3 [27,44]. The spinel $Li[Ni_{0.5}Mn_{1.5}]O_4$ progressively converted into the disordered rock-salt-type $[Li_xTM_{(1-x)}]O$ and the ordered monoclinic layered LLNMO when the temperature was increased from 600 to 700 °C. Noticeably, the sXRD pattern contained several additional weak reflections close to those from the main layered LLNMO phase, which were assigned to the spinel $Li[Ni_{0.5}Mn_{1.5}]O_4$. The remaining spinel $LiTM_2O_4$ at 700 °C was probably associated with (1) unreacted Li species on the surface of crystals or (2) the relatively low temperature (≤ 700 °C).

In contrast, when the temperature reached 750 °C, there were almost no reflections in the in situ HT-sXRD patterns belonging to the spinel $LiTM_2O_4$ and the defective $Li_{2-x}CO_3$, possibly because Li_2CO_3 decomposition was complete (see Figs. 4d and h). These results also indicated that the activation energy barrier for the transition from a Li-containing spinel to a Li-rich layered phase could easily be surmounted at higher temperatures (≥ 750 °C). The apparent crystallinity of the $Li[Ni_{0.5}Mn_{1.5}]O_4$ intermediate (66(2)%) under 750 °C was close to that of the spinel $LiTM_2O_4$ phase formed at 650 and 725 °C (i.e., 65(2)% and 66(3)%), probably because the phase transition from spinel $Li[Ni_{0.5}Mn_{1.5}]O_4$ to layered $Li[Li_{0.2}Ni_{0.2}Mn_{0.6}]O_2$ took place rapidly, allowing no time for Li

$[Ni_{0.5}Mn_{1.5}]O_4$ growth. Therefore, very rapid lithiation kinetics plays a crucial role in the formation of layered LLNMO.

Fig. 5 displays the relative phase fractions of the mixtures during annealing. With an increase in temperature from about 600 °C onward, the weight fraction of the Li-free spinel phase TM_3O_4 ($Fd\bar{3}m$) gradually decreased from around 60(5) wt% to 2(2) wt% (see Fig. 5a), while the percentage of Li-containing spinel $LiTM_2O_4$ ($Fd\bar{3}m$) intermediate increased to approximately 55(5) wt%, accompanied by the disintegration of lithium sources. Hereafter, a phase transition from the Li-containing spinel structure to the Li-containing rock-salt structure and a layered structure occurred. After phase transformation, the relative percentage of the layered LLNMO phase and the rock-salt-type $[Li_xTM_{(1-x)}]O$ phase rose to approximately 71(5) and 15(5) wt%, respectively.

Fig. 5b presents the evolution of the weight fractions of various phases during heating to 700 °C, showing that spinel TM_3O_4 and Li_2CO_3 reacted to yield a Li-containing rock-salt-type phase (~65(5) wt%) and defective lithium carbonate (~35(5) wt%) upon calcination. As the reaction time increased, the fraction of both phases profoundly diminished, resulting in a greater percentage of the Li-rich layered phase (~77(5) wt%) and revealing the successive transformation from the rock-salt-type phase to the layered LLNMO. The changes in the phase fractions at 725 °C (Fig. 5c) were similar to those at 750 °C (Fig. 5d). The structural evolution from a Li-free spinel phase to a Li-containing spinel/rock-salt-type phase and eventually to a Li-rich layered phase was clearly observed. Compared to the phase fraction evolution at 725 °C, almost no $Li_{2-x}CO_3$ was detected when the temperature increased to 750 °C, suggesting the completion of Li_2CO_3 decomposition. Consequently, the weight fraction of layered LLNMO (~90(5) wt%) at 750 °C was higher than that of LLNMO obtained at 725 °C (~83(5) wt%).

The in situ HT-sXRD results unambiguously demonstrated that the chemical reaction between Li-free precursor and Li/O species during the synthesis of LLNMO is a multistep reaction, which is rate-limited by the formation of Li-containing spinel/rock-salt-type intermediates or the disintegration of Li sources. Thermodynamically, various temperature scales are closely tied to different time scales. A low temperature takes the reaction system far away from thermal equilibrium. As the temperature increases, the time required to reach equilibrium decreases exponentially. The activation energy barrier from a Li-containing spinel/rock-salt-type intermediate to a Li-rich layered oxide could hinder the thermodynamic phase transition at a low temperature. On the other hand, the high-temperature lithiation reaction is also determined by the decomposition of Li species, which provide the desired Li/O species for the phase transformation from Li-poor intermediates to Li-rich oxides. For example, the Li-containing spinel $LiTM_2O_4$ intermediate was formed at 650, 725 and 750 °C when a mixture of Li_2CO_3 (98 wt%) and LiOH (2 wt %) was used as the Li source, but there was no spinel $LiTM_2O_4$ intermediate at 700 °C, because of the high decomposition temperature (723 °C) of Li_2CO_3 (see Fig. 4). Therefore, it is often difficult to observe the thermodynamically driven formation of monoclinic layered LLNMO at low temperatures (< 700 °C) or with a short calcination time. Together, changes in the heating temperature or precursor type affected the lithiation reaction pathways and thereby the chemical and phase composition of the final product. Nevertheless, the formation of Li-rich cathode materials during the high-temperature solid-state reaction was

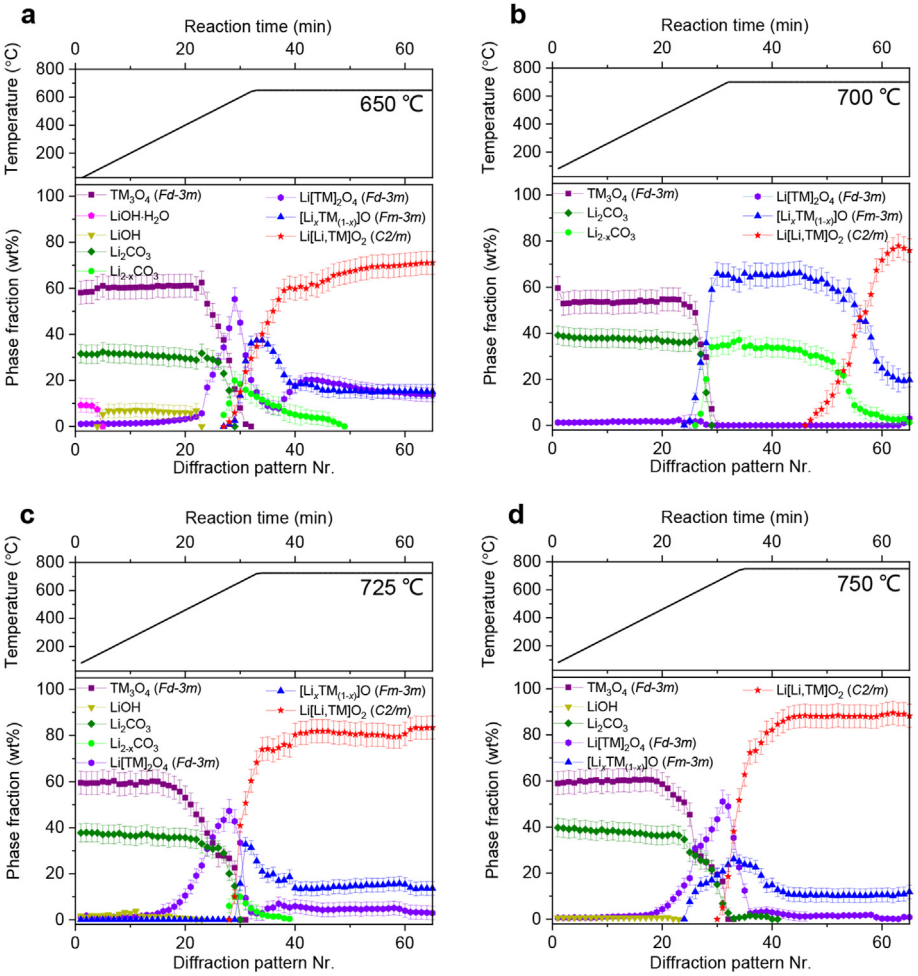

Fig. 5. A quantitative analysis of the weight fractions of various phases obtained from Rietveld refinement against in situ HT-sXRD data at (a) 650, (b) 700, (c) 725, and (d) 750 °C.

thermodynamically favored. When a mixture of different precursors with an appropriate amount of Li source was calcined at high temperature (e.g., 850 °C) for a long time (e.g., 12 h), the reactants always converted into Li-rich layered oxides.

Recently, Guo et al. reported a stable high-nickel cathode with dense amorphous Li_2CO_3 on the particle surface [46]. The assembled coin cell with this modified cathode delivered a good capacity retention of 90.4% after 100 cycles. Xie et al. suggested that the rational design of a spinel/layered heterostructure in Li-rich cathode materials could effectively improve the rate capability because the 3D diffusion channel of the spinel structure permits fast Li-ion transport, and the layered structure guarantees high storage capacity [47]. Thus, uncovering this lithiation mechanism provides new insight into the preparation of spinel/layered heterostructured Li-rich oxides and the fabrication of an amorphous Li_2CO_3 surface coating for a Li-rich layered oxide cathode with long durability.

To gain further valuable insights into the phase transformation from the fully disordered rock-salt-type $[Li_xTM_{(1-x)}]O$ phase (*Fm* $\bar{3}$ *m*) to the monoclinic layered Li[Li,TM]O_2 phase (*C2/m*), the changes with time in the lattice parameters of both phases at 700 °C were further analyzed using the Rietveld refinement method, as shown in Fig. S8a. Surprisingly, the parameter *a* of the cubic rock-salt unit cell was reduced from ~4.2823(5) to ~4.1813(5) Å, which was in good agreement with the reflections shifting to higher scattering angles, demonstrating strong lattice shrinkage in the Li-containing rock-salt structure. This shrinkage can be interpreted as a reordering from a random distribution of the larger Li ions and the TM ions on one site in the ccp oxygen framework, which required more space than in the evolving high-temperature phase with its a higher degree of order; this reordering occurred by the formation of alternating planes with either only Li or only TM cations in separate layers (r_{Li^+} = 0.76 Å, $r_{Ni^{2+}}$ = 0.69 Å, $r_{Mn^{4+}}$ = 0.53 Å) [48]. The reaction of the disordered rock-salt-type phase with Li/O species occurred slowly at 700 °C, implying that the transformation from the fully disordered rock salt to the ordered layered structure was kinetically hindered. Significantly, all the parameters (*a*, *b*, and *c*) of the monoclinic layered structure were reduced during the transition from disordered rock-salt-type to ordered layered phase, indicating that the long-range ordering of cations in the ccp oxygen lattice resulted in a reduction of the average lattice parameters of the layered structure.

Fig. S8b shows a structural model for illustrating the transformation from rock-salt structure (*Fm*$\bar{3}$*m*) to monoclinic layered structure (*C2/m*). The rhombohedral layered structure (*R*$\bar{3}$*m*) can be formed by alternating Li and TM ions in a rock-salt-type unit cell of doubled cell parameter where the ordering occurs in the planes along the $[111]_r$ axis in the rhombohedral setting, which is $[001]_h$ in the hexagonal setting. In the rhombohedral layered structure (*R*$\bar{3}$*m*), the TM plane is almost fully occupied by TM cations. In contrast, a surfeit of Li ions can be located on octahedral sites in the TM layer in the monoclinic layered structure (*C2/m*), forming a honeycomb superstructure (i.e. in-plane Li/TM ordering).

To investigate whether the discovered high-temperature lithiation reaction mechanism has high relevance for the synthesis of Na/K-containing layered oxides, HT-sXRD was conducted to track the structural evolution of a mixture of $Mn[Ni_{0.75}Mn_{1.25}]O_4$ (TM_3O_4) and carbonate precursor (i.e., Na_2CO_3 and K_2CO_3) during heat treatment

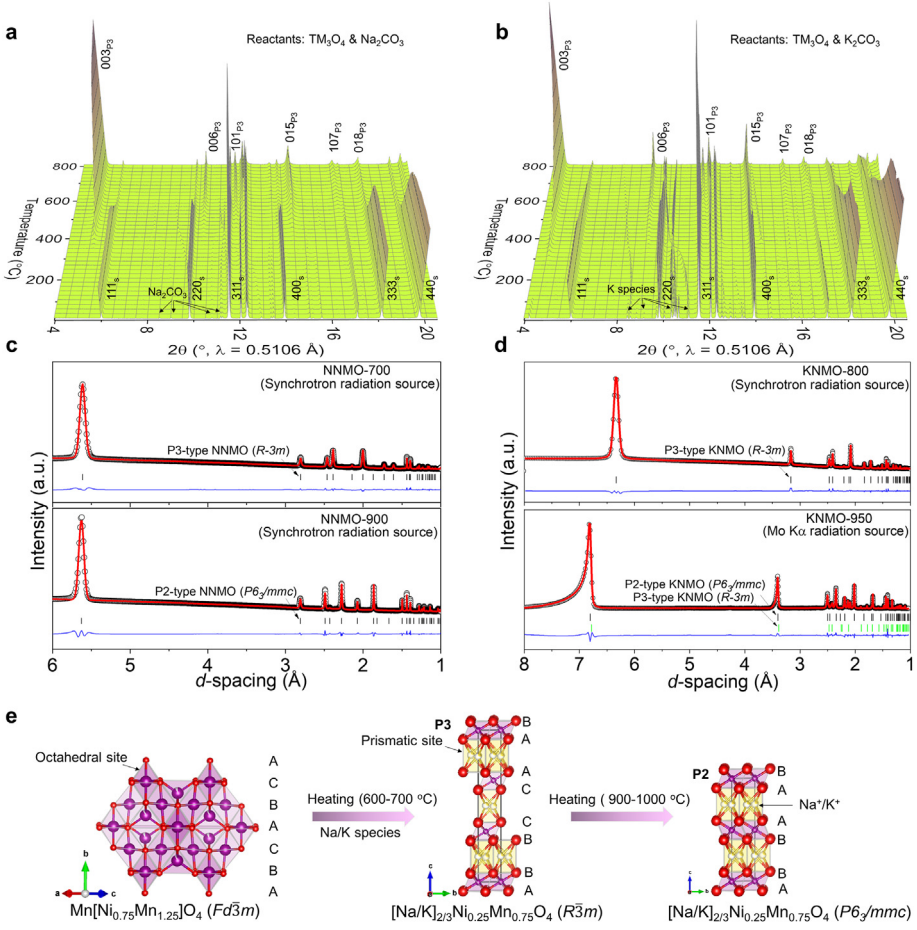

Fig. 6. In situ HT-sXRD patterns of a mixture of (a) TM_3O_4 together with Na_2CO_3, (b) TM_3O_4 and K_2CO_3 during solid-state synthesis between 25 and 800 °C; (c) Rietveld refinement results against sXRD patterns of NNMO-700 and NNMO-900; (d) Rietveld refinement results against XRD patterns of KNMO-800 and KNMO-950; (e) illustration of the Na-ion/K-ion insertion-induced structural evolution of TM_3O_4 during heating.

(25–800 °C). As presented in Fig. 6a, the reflections in the in situ HT-sXRD patterns of Na_2CO_3 gradually disappeared until the temperature was ~600 °C. Simultaneously, a new set of reflections at 003_{P3}, 101_{P3}, 107_{P3}, and 018_{P3} emerged, which were indexed based on a P3-type layered structure ($R\bar{3}m$) and indicated the formation of P3-type $Na_{2/3}Ni_{0.25}Mn_{0.75}O_2$ (i.e. $\frac{1}{3}\ Na_2CO_3 + \frac{1}{3}\ Mn[Ni_{0.75}Mn_{1.25}]O_4 + \frac{1}{6}\ O_2 \xrightarrow{\Delta} Na_{2/3}Ni_{0.25}Mn_{0.75}O_2 + \frac{1}{3}\ CO_2$, see Fig. S9). With a further increase in temperature to 800 °C, the integrated intensity of all the reflections of P3-type $Na_{2/3}Ni_{0.25}Mn_{0.75}O_2$ (NNMO) increased continuously, implying the ongoing formation of such crystals upon calcination. The maximum temperature for these in situ HT-sXRD experiments was 800 °C. To obtain the expected thermodynamically stable P2-type layered phase, the reactants were heated to 900 °C for 12 h ex situ under an air atmosphere. For comparison, the mixture was also calcined to 700 °C for 12 h. The resulting powders were respectively designated NNMO-900 and NNMO-700. Rietveld refinement results against sXRD data collected at room temperature (Fig. 6c) confirmed that NNMO-900 possessed a P2-type layered phase with the space group of $P6_3/mmc$, while NNMO-700 remained in a P3-type layered phase ($R\bar{3}m$), further verifying that the P3-type layered phase was a metastable phase and confirming that 700 °C was not sufficient to activate the transition into the P2-type structure (see Fig. 6e).

The in situ HT-sXRD patterns of the TM_3O_4 and K_2CO_3 compounds during heating are shown in Fig. 6b. Comparatively, the K-free spinel TM_3O_4 phase progressively converted to a P3-type layered $K_{2/3}Ni_{0.25}Mn_{0.75}O_2$ as a result of K/O incorporation when the temperature was increased to around 800 °C (see Fig. S10). Note that K_2CO_3 rapidly decomposed or reacted into several K species at elevated temperatures, but these could not be identified by powder diffraction data only. The reactants TM_3O_4 and K_2CO_3 were also heated to 800 °C or 950 °C for 12 h, and the obtained samples were designated KNMO-800 and KNMO-950. All the reflections in the sXRD pattern of KNMO-800 collected at room temperature were indexed according to a P3-type layered structure ($R\bar{3}m$; see Fig. 6d). KNMO-950 was composed of a mixture of P3-type ($R\bar{3}m$) and P2-type layered ($P6_3/mmc$) phases. The phase composition was estimated to be 75(6) wt% for the P2-type KNMO and 25(4) wt% for the P3-type KNMO-950. Rietveld refinement results showed that the lattice parameters a and c of the P3-type layered KNMO-800 ($R\bar{3}m$) were, respectively, 2.8762(5) and 19.0016(5) Å, which were higher than those of P3-type layered NNMO-700 (2.8745(5) Å and 16.8334(5) Å), reflecting that KNMO-800 had larger interlayer spacing than NNMO-700 due to the larger ionic radius of potassium ($r_{Na^+} = 1.02$ Å, $r_{K^+} = 1.38$ Å).

Compared to these high-temperature solid-state reactions, the Li ions strongly preferred to occupy the tetrahedral sites within the ccp oxygen lattice at low Li content or low temperature, forming a Li-containing spinel phase such as $Li[Ni_{0.5}Mn_{1.5}]O_4$ ($Fd\bar{3}m$). The Na and K ions tended to migrate to the prismatic sites, producing P3- or P2-type layered phases such as $Na_{2/3}Ni_{0.25}Mn_{0.75}O_2$ and $K_{2/3}Ni_{0.25}Mn_{0.75}O_2$ ($R\bar{3}m$) upon annealing. Such site preferences probably precluded the generation of Na-containing spinel, K-containing spinel, or O3-type layered intermediates during the synthesis of Na-defective layered oxides or K-defective layered oxides.

3. Conclusion

In summary, Li-ion/Na-ion/K-ion insertion into an alkali-free host structure during thermal treatment was systematically investigated using in situ high-resolution HT-sXRD experiments on a time scale of minutes. A Li^+/H^+-ion exchange reaction was observed at a relatively low temperature (~500 °C) during the preparation of Li-rich layered LLNMO via a hydroxide coprecipitation route. The carbonate precursor induced a transformation from the rhombohedral structure ($R\bar{3}c$) to the fully disordered Li-containing rock-salt-type $[Li_xTM_{1-x}]O$ ($0 \leq x \leq 0.5$) ($Fm\bar{3}m$) and finally to the monoclinic layered LLNMO ($C2/m$) as Li/O ions were incorporated upon annealing. When an appropriate amount of lithium source ($LiOH{\cdot}H_2O$ and/or Li_2CO_3) and Li-free spinel TM_3O_4 oxide came together at high temperatures, various pathways of LLNMO formation were unveiled, which were strongly dependent on the decomposition of Li species. These findings offer new insights for achieving the commercial fabrication of layered Li-rich electrode materials. Furthermore, the in situ and ex situ sXRD results suggest that the Na- and K-free spinel structure ($Fd\bar{3}m$) would transform to a metastable P3-type layered structure ($R\bar{3}m$) and eventually to a thermodynamically stable P2-type layered structure ($P6_3/mmc$) at high temperature as a result of Na or K and O incorporation. Understanding the synthesis methods of P2-type and P3-type Na- or K-layered structures can help to synthesize advanced electrode materials with a desirable crystallographic structure for high-performance Na-ion and K-ion batteries.

Author contribution

W.H. conceived the idea and discussed with X.Y., L.L, S.W., M.K., H.E and S.I.; W.H. and S.W. carried out the preparation experiments; W.H., N.P.M.C. and V.B. performed the synchrotron based and laboratory X-ray diffraction measurements; the data were analyzed by X.Y., W.H. and S.W.; X.Y., W.H., and S.W wrote the preliminary draft with input from S.I; all authors revised the manuscript and have given the approval to the final version of the manuscript.

Notes

The authors declare they have no competing financial interest.

Conflict of interest

The authors declared that they have no conflicts of interest to this work.

Acknowledgements

W. H. acknowledges the National Natural Science Foundation of China (grant no. 22108218) and "Young Talent Support Plan" of Xi'an Jiaotong University (71211201010723). This work was financially supported by the China Postdoctoral Science Foundation (Grant No. 2021M693813), Guangxi Science and Technology Base and Talents Special Project (Grant No. AD21159007), the Natural Science Foundation of Guangxi (Grant No. 2020GXNSFBA297029), the Foundation of Key Laboratory of New Processing Technology for Nonferrous Metal & Materials, Ministry of Education/Guangxi Key Laboratory of Optical and Electronic Materials and Devices, Guilin University of Technology (Contract No. 20AA-13), the Foundation of Guilin University of Technology (GLUTQDJJ2020003), and High Level Innovation Team and Outstanding Scholar Program of Guangxi Institutes. We acknowledge DESY (Hamburg, Germany), a member of the Helmholtz Association HGF, and Paul Scherrer Institut (Villigen PSI, Switzerland) for the provision of experimental facilities. We also thank the Instrument Analysis Center of Xi'an Jiao Tong University for the assistance test. This work contributes to the research performed at CELEST (Center for Electrochemical Energy Storage Ulm-Karlsruhe) and was supported by the German Research Foundation (DFG) under Project ID 390874152 (POLiS Cluster of Excellence).

Appendix A. Supplementary data

Supplementary data to this article can be found online at https://doi.org/10.1016/j.esci.2022.02.007.

References

[1] J.E. Fröch, A. Bahm, M. Kianinia, Z. Mu, V. Bhatia, S. Kim, J.M. Cairney, W. Gao, C. Bradac, I. Aharonovich, M. Toth, Versatile direct-writing of dopants in a solid state host through recoil implantation, Nat. Commun. 11 (2020) 5039.

[2] L.J. Rogers, K.D. Jahnke, T. Teraji, L. Marseglia, C. Müller, B. Naydenov, H. Schauffert, C. Kranz, J. Isoya, L.P. McGuinness, F. Jelezko, Multiple intrinsically identical single-photon emitters in the solid state, Nat. Commun. 5 (2014) 4739.

[3] M. Huang, A. Jun Tan, F. Büttner, H. Liu, Q. Ruan, W. Hu, C. Mazzoli, S. Wilkins, C. Duan, J.K.W. Yang, G.S.D. Beach, Voltage-gated optics and plasmonics enabled by solid-state proton pumping, Nat. Commun. 10 (2019) 5030.

[4] M.J. McDermott, S.S. Dwaraknath, K.A. Persson, A graph-based network for predicting chemical reaction pathways in solid-state materials synthesis, Nat. Commun. 12 (2021) 3097.

[5] Y. Shen, G. Xue, Y. Dai, S.M. Quintero, H. Chen, D. Wang, F. Miao, F. Negri, Y. Zheng, J. Casado, Normal & reversed spin mobility in a diradical by electron-vibration coupling, Nat. Commun. 12 (2021) 6262.

[6] A. Ramirez, X. Gong, M. Caglayan, S.-A.F. Nastase, E. Abou-Hamad, L. Gevers, L. Cavallo, A. Dutta Chowdhury, J. Gascon, Selectivity descriptors for the direct hydrogenation of CO_2 to hydrocarbons during zeolite-mediated bifunctional catalysis, Nat. Commun. 12 (2021) 5914.

[7] Y. Yang, P.-P. Wang, Z.-C. Zhang, H.-L. Liu, J. Zhang, J. Zhuang, X. Wang, Nanowire membrane-based nanothermite: towards processable and tunable interfacial diffusion for solid state reactions, Sci. Rep. 3 (2013) 1694.

[8] M. Liu, C. Wang, C. Zhao, E. van der Maas, K. Lin, V.A. Arszelewska, B. Li, S. Ganapathy, M. Wagemaker, Quantification of the Li-ion diffusion over an interface coating in all-solid-state batteries via NMR measurements, Nat. Commun. 12 (2021) 5943.

[9] Y. Chen, Z. Wang, X. Li, X. Yao, C. Wang, Y. Li, W. Xue, D. Yu, S.Y. Kim, F. Yang, A. Kushima, G. Zhang, H. Huang, N. Wu, Y.-W. Mai, J.B. Goodenough, J. Li, Li metal deposition and stripping in a solid-state battery via coble creep, Nature 578 (2020) 251–255.

[10] H. Huo, J. Gao, N. Zhao, D. Zhang, N.G. Holmes, X. Li, Y. Sun, J. Fu, R. Li, X. Guo, X. Sun, A flexible electron-blocking interfacial shield for dendrite-free solid lithium metal batteries, Nat. Commun. 12 (2021) 176.

[11] S. Wang, W. Hua, A. Missyul, M.S.D. Darma, A. Tayal, S. Indris, H. Ehrenberg, L. Liu, M. Knapp, Kinetic control of long-range cationic ordering in the synthesis of layered Ni-rich oxides, Adv. Funct. Mater. 31 (2021) 2009949.

[12] T. Gao, X. Ji, S. Hou, X. Fan, X. Li, C. Yang, F. Han, F. Wang, J. Jiang, K. Xu, C. Wang, Thermodynamics and kinetics of sulfur cathode during discharge in $MgTFSI_2$-DME electrolyte, Adv. Mater. 30 (2018) 1704313.

[13] I.P. Parkin, Solid state metathesis reaction for metal borides, silicides, pnictides and chalcogenides: ionic or elemental pathways, Chem. Soc. Rev. 25 (1996) 199–207.

[14] X. Zhong, M. Oubla, X. Wang, Y. Huang, H. Zeng, S. Wang, K. Liu, J. Zhou, L. He, H. Zhong, N. Alonso-Vante, C.-W. Wang, W.-B. Wu, H.-J. Lin, C.-T. Chen, Z. Hu, Y. Huang, J. Ma, Boosting oxygen reduction activity and enhancing stability through structural transformation of layered lithium manganese oxide, Nat. Commun. 12 (2021) 3136.

[15] Y. Tokura, N. Nagaosa, Orbital physics in transition-metal oxides, Science 288 (2000) 462–468.

[16] V. Kalinin Sergei, A. Spaldin Nicola, Functional ion defects in transition metal oxides, Science 341 (2013) 858–859.

[17] C.N.R. Rao, A.K. Cheetham, Giant magnetoresistance in transition metal oxides, Science 272 (1996) 369–370.

[18] J. Suntivich, K.J. May, H.A. Gasteiger, J.B. Goodenough, Y. Shao-Horn, A perovskite oxide optimized for oxygen evolution catalysis from molecular orbital principles, Science 334 (2011) 1383–1385.

[19] Q. Yin, J.M. Tan, C. Besson, Y.V. Geletii, D.G. Musaev, A.E. Kuznetsov, Z. Luo, K.I. Hardcastle, C.L. Hill, A fast soluble carbon-free molecular water oxidation catalyst based on abundant metals, Science 328 (2010) 342–345.

[20] G. Chen, W. Zhou, D. Guan, J. Sunarso, Y. Zhu, X. Hu, W. Zhang, Z. Shao, Two orders of magnitude enhancement in oxygen evolution reactivity on amorphous $Ba_{0.5}Sr_{0.5}Co_{0.8}Fe_{0.2}O_{3-\delta}$ nanofilms with tunable oxidation state, Sci. Adv. 3 (2017), e1603206.

[21] M. Bianchini, J. Wang, R.J. Clement, B. Ouyang, P. Xiao, D. Kitchaev, T. Shi, Y. Zhang, Y. Wang, H. Kim, M. Zhang, J. Bai, F. Wang, W. Sun, G. Ceder, The interplay between thermodynamics and kinetics in the solid-state synthesis of layered oxides, Nat. Mater. 19 (2020) 1088–1095.

[22] Y. Xiao, N.M. Abbasi, Y.F. Zhu, S. Li, S.J. Tan, W. Ling, L. Peng, T. Yang, L. Wang, X.D. Guo, Y.X. Yin, H. Zhang, Y.G. Guo, Layered oxide cathodes promoted by structure modulation Technology for sodium-ion batteries, Adv. Funct. Mater. 30 (2020) 2001334.

[23] Z. Yang, L. Mu, D. Hou, M.M. Rahman, Z. Xu, J. Liu, D. Nordlund, C.J. Sun, X. Xiao, F. Lin, Probing dopant redistribution, phase propagation, and local chemical changes in the synthesis of layered oxide battery cathodes, Adv. Energy Mater. 11 (2021) 2002719.

[24] W.C. Zhang, Y.J. Liu, Z.P. Guo, Approaching high-performance potassium-ion batteries via advanced design strategies and engineering, Sci. Adv. 5 (2019), eaav7412.

[25] W. Hua, S. Wang, K. Wang, A. Missyul, Q. Fu, M.S. Dewi Darma, H. Li, V. Baran, L. Liu, C. Kübel, J.R. Binder, M. Knapp, H. Ehrenberg, S. Indris, Li^+/Na^+ ion exchange in layered $Na_{2/3}(Ni_{0.25}Mn_{0.75})O_2$: a simple and fast way to synthesize O_3/O_2-type layered oxides, Chem. Mater. 33 (2021) 5606–5617.

[26] D. Luo, S. Fang, Y. Tamiya, L. Yang, S.I. Hirano, Countering the segregation of transition-metal ions in $LiMn_{1/3}Co_{1/3}Ni_{1/3}O_2$ cathode for ultralong life and high-energy Li-ion batteries, Small 12 (2016) 4421–4430.

[27] W. Hua, S. Wang, M. Knapp, S.J. Leake, A. Senyshyn, C. Richter, M. Yavuz, J.R. Binder, C.P. Grey, H. Ehrenberg, S. Indris, B. Schwarz, Structural insights into the formation and voltage degradation of lithium- and manganese-rich layered oxides, Nat. Commun. 10 (2019) 5365.

[28] Y. Pei, C.Y. Xu, Y.C. Xiao, Q. Chen, B. Huang, B. Li, S. Li, L. Zhen, G. Cao, Phase transition induced synthesis of layered/spinel heterostructure with enhanced electrochemical properties, Adv. Funct. Mater. 27 (2017) 1604349.

[29] J. Bai, W. Sun, J. Zhao, D. Wang, P. Xiao, J.Y.P. Ko, A. Huq, G. Ceder, F. Wang, Kinetic pathways templated by low-temperature intermediates during solid-state synthesis of layered oxides, Chem. Mater. 32 (2020) 9906–9913.

[30] J. Lee, D.A. Kitchaev, D.H. Kwon, C.W. Lee, J.K. Papp, Y.S. Liu, Z. Lun, R.J. Clement, T. Shi, B.D. McCloskey, J. Guo, M. Balasubramanian, G. Ceder, Reversible Mn^{2+}/Mn^{4+} double redox in lithium-excess cathode materials, Nature 556 (2018) 185–190.

[31] J. Hong, W.E. Gent, P. Xiao, K. Lim, D.-H. Seo, J. Wu, P.M. Csernica, C.J. Takacs, D. Nordlund, C.-J. Sun, K.H. Stone, D. Passarello, W. Yang, D. Prendergast, G. Ceder, M.F. Toney, W.C. Chueh, Metal-oxygen decoordination stabilizes anion redox in Li-rich oxides, Nat. Mater. 18 (2019) 256–265.

[32] S. Saha, G. Assat, M.T. Sougrati, D. Foix, H. Li, J. Vergnet, S. Turi, Y. Ha, W. Yang, J. Cabana, G. Rousse, A.M. Abakumov, J.-M. Tarascon, Exploring the bottlenecks of anionic redox in Li-rich layered sulfides, Nat. Energy 4 (2019) 977–987.

[33] F. Wang, J. Bai, Synthesis and processing by design of high-nickel cathode materials, Batteries Supercaps 5 (2022), e202100174.

[34] T. Liu, L. Yu, J. Lu, T. Zhou, X. Huang, Z. Cai, A. Dai, J. Gim, Y. Ren, X. Xiao, M.V. Holt, Y.S. Chu, I. Arslan, J. Wen, K. Amine, Rational design of mechanically robust Ni-rich cathode materials via concentration gradient strategy, Nat. Commun. 12 (2021) 6024.

[35] D. Wang, R. Kou, Y. Ren, C.J. Sun, H. Zhao, M.J. Zhang, Y. Li, A. Huq, J.Y.P. Ko, F. Pan, Y.K. Sun, Y. Yang, K. Amine, J. Bai, Z. Chen, F. Wang, Synthetic control of kinetic reaction pathway and cationic ordering in high-Ni layered oxide cathodes, Adv. Mater. 29 (2017) 1606715.

[36] W.-S. Yoon, O. Haas, S. Muhammad, H. Kim, W. Lee, D. Kim, D.A. Fischer, C. Jaye, X.-Q. Yang, M. Balasubramanian, K.-W. Nam, In situ soft XAS study on nickel-based layered cathode material at elevated temperatures: a novel approach to study thermal stability, Sci. Rep. 4 (2014) 6827.

[37] M.J. Zhang, G. Teng, Y.K. Chen-Wiegart, Y. Duan, J.Y.P. Ko, J. Zheng, J. Thieme, E. Dooryhee, Z. Chen, J. Bai, K. Amine, F. Pan, F. Wang, Cationic ordering coupled to reconstruction of basic building units during synthesis of high-Ni layered oxides, J. Am. Chem. Soc. 140 (2018) 12484–12492.

[38] Y.-Y. Hu, Z. Liu, K.-W. Nam, O.J. Borkiewicz, J. Cheng, X. Hua, M.T. Dunstan, X. Yu, K.M. Wiaderek, L.-S. Du, K.W. Chapman, P.J. Chupas, X.-Q. Yang, C.P. Grey, Origin of additional capacities in metal oxide lithium-ion battery electrodes, Nat. Mater. 12 (2013) 1130–1136.

[39] Y. Zhu, J.W. Wang, Y. Liu, X. Liu, A. Kushima, Y. Liu, Y. Xu, S.X. Mao, J. Li, C. Wang, J.Y. Huang, In situ atomic-scale imaging of phase boundary migration in $FePO_4$ microparticles during electrochemical lithiation, Adv. Mater. 25 (2013) 5461–5466.

[40] P.S. Maram, S.V. Ushakov, R.J.K. Weber, C.J. Benmore, A. Navrotsky, Probing disorder in pyrochlore oxides using in situ synchrotron diffraction from levitated solids–A thermodynamic perspective, Sci. Rep. 8 (2018) 10658.

[41] J. Gustafson, M. Shipilin, C. Zhang, A. Stierle, U. Hejral, U. Ruett, O. Gutowski, P.A. Carlsson, M. Skoglundh, E. Lundgren, High-energy surface X-ray diffraction for fast surface structure determination, Science 343 (2014) 758–761.

[42] A. Johannes, D. Salomon, G. Martinez-Criado, M. Glaser, A. Lugstein, C. Ronning, Operando X-ray imaging of nanoscale devices: composition, valence, and internal electrical fields, Sci. Adv. 3 (2017), eaao4044.

[43] W. Hua, K. Wang, M. Knapp, B. Schwarz, S. Wang, H. Liu, J. Lai, M. Müller, A. Schökel, A. Missyul, D. Ferreira Sanchez, X. Guo, J.R. Binder, J. Xiong, S. Indris, H. Ehrenberg, Chemical and structural evolution during the synthesis of layered $Li(Ni,Co,Mn)O_2$ oxides, Chem. Mater. 32 (2020) 4984–4997.

[44] W. Hua, M. Chen, B. Schwarz, M. Knapp, M. Bruns, J. Barthel, X. Yang, F. Sigel, R. Azmi, A. Senyshyn, A. Missiul, L. Simonelli, M. Etter, S. Wang, X. Mu, A. Fiedler, J.R. Binder, X. Guo, S. Chou, B. Zhong, S. Indris, H. Ehrenberg, Lithium/oxygen incorporation and microstructural evolution during synthesis of Li-rich layered $Li[Li_{0.2}Ni_{0.2}Mn_{0.6}]O_2$ oxides, Adv. Energy Mater. 9 (2019) 1803094.

[45] J. Zhao, W. Zhang, A. Huq, S.T. Misture, B. Zhang, S. Guo, L. Wu, Y. Zhu, Z. Chen, K. Amine, F. Pan, J. Bai, F. Wang, In situ probing and synthetic control of cationic ordering in Ni-rich layered oxide cathodes, Adv. Energy Mater. 7 (2017) 1601266.

[46] H. Sheng, X.H. Meng, D.D. Xiao, M. Fan, W.P. Chen, J. Wan, J. Tang, Y.G. Zou, F. Wang, R. Wen, J.L. Shi, Y.G. Guo, Air-stable high-nickel cathode with reinforced electrochemical performance enabled by convertible amorphous Li_2CO_3 modification, Adv. Mater 35 (2022), e2108947.

[47] H. Xie, J. Cui, Z. Yao, X. Ding, Z. Zhang, D. Luo, Z. Lin, Revealing the role of spinel phase on Li-rich layered oxides: a review, Chem. Eng. J. 427 (2022) 131978.

[48] R.D. Shannon, Revised effective ionic radii and systematic studies of interatomic distances in halides and chalcogenides, Acta Crystallogr. A 32 (1976) 751–767.